SCIENCE CHINA
Life Sciences

• RESEARCH PAPER •

September 2012 Vol.55 No.9: 782–787
doi: 10.1007/s11427-012-4361-4

An *in vivo* study with an MRI tracer method reveals the biophysical properties of interstitial fluid in the rat brain

HAN HongBin[1,2*], LI Kai[1,2], YAN JunHao[3], ZHU Kai[1,2] & FU Yu[2,4]

[1]*Department of Radiology, Peking University Third Hospital, Beijing 100191, China;*
[2]*Beijing Key Laboratory of Magnetic Resonance Imaging Device and Technique, Beijing 100191, China;*
[3]*Department of Anatomy, Histology and Embryology, Peking University Health Science Center, Beijing 100083, China;*
[4]*Department of Neurology, Peking University Third Hospital, Beijing 100191, China*

Received June 15, 2012; accepted July 5, 2012

The nature of brain interstitial fluid (ISF) has long been a subject of controversy. Most of the previous studies on brain ISF were carried out *in vitro*. In the present study, a novel method was developed to characterize ISF in the living rat brain by magnetic resonance (MR) imaging using gadolinium-diethylenetriaminepentaacetic acid (Gd-DTPA) as a tracer. Sprague Dawley rats (n=8) were subjected to MR scanning before and after the introduction of Gd-DTPA into the caudate nucleus. A one-way drainage of brain ISF was demonstrated on the dynamic MR images. According to the traditional diffusion model, the diffusion and clearance rate constants of the tracer within brain extracellular space (ECS) were derived as $(3.38\pm1.07)\times10^{-4}$ mm^2 s^{-1} and $(7.60\pm4.18)\times10^{-5}$ s^{-1}. Both diffusion and bulk flow contributed to the drainage of ISF from the caudate nucleus, which demonstrated an ISF-cerebrospinal fluid confluence in the subarachnoid space at the lateral and ventral surface of the brain cortex at 3 h after the injection. By using this newly developed method, the brain ECS and ISF can be quantitatively measured simultaneously in the living brain, which will enhance the understanding of ISF and improve the efficiency of drug therapy via the brain interstitium.

Gd-DTPA, extracellular space, quantitative imaging, diffusion, interstitial fluid

Citation: Han H B, Li K, Yan J H, *et al*. An *in vivo* study with an MRI tracer method reveals the biophysical properties of interstitial fluid in the rat brain. Sci China Life Sci, 2012, 55: 782−787, doi: 10.1007/s11427-012-4361-4

Neurons are bathed by the interstitial fluid (ISF) within the brain extracellular space (ECS) which forms the microenvironment of the central nervous system (CNS). The origin, drainage and clearance of brain ISF have been the subject of speculation and controversy for more than 100 years [1]. Most of the previous methods to study ISF drainage were performed *in vitro* and could not provide the biophysical properties of the brain ECS simultaneously. Comparatively, with several *in vivo* quantitative methods, there is less controversy on the biophysical structure of the brain ECS, which has been recognized as a system of intercellular communication channels containing many bioactive substances including nutrients, metabolites, chemical ions, and neurotransmitters [2]. Although the results obtained with real-time iontophoresis (RTI) method have formed the basis for much of our present understanding of the diffusion properties of the brain ECS [3–5], they provided the data only for very small volumes of living brain tissue [2] and information on the spatial distribution and drainage process of ISF was not available.

There is currently great potential to exploit knowledge of the brain ECS and ISF so as to treat brain diseases more effectively. Recently, with positive evidence for convection enhanced delivery (CED) [6] and simple diffusion delivery

*Corresponding author (email: hanhongbin@bjmu.edu.cn)

(SDD) [7], local intracranial injection via the brain ECS has become an appealing drug delivery method for the treatment of CNS diseases [8]. The methodology to monitor the real-time distribution and the clearance process after drug administration via the brain ECS is essential to enhance therapeutic efficacy [9]. Therefore, knowledge of the brain ECS and ISF is urgently required for future clinical practice. In the present study, a novel method is developed to quantitatively measure both the brain ECS and ISF in the living brain by magnetic resonance imaging (MRI) using gadolinium-diethylenetriaminepentaacetic acid (Gd-DTPA) as a tracer.

1 Materials and methods

1.1 Phantom experiments for establishing the linear relationship between *ΔSI* and Gd-DTPA concentration

Gd-DTPA (Magnevist; Bayer Schering Pharma AG, Berlin, Germany) was diluted with double distilled water in tubes. Eleven samples of a concentration gradient were prepared; concentrations of sample solutions were over the range of 0–1 mmol L^{-1}. Magnetic resonance (MR) scanning was performed at 37°C by submerging tubes in a water bath when they were placed in the scanner. Parameters for the imaging sequence were as follows: echo time (TE)=3.7 ms, repetition time (TR)=1500 ms, flip angle (FA)=9°, inversion time (TI)=900 ms, slice thickness (SL)=1 mm, field of view (FOV)=267 mm, voxel=0.5 mm×0.5 mm×0.5 mm. Signal intensity (*SI*) was measured by selecting the region of interest (ROI) of every tube in the center of the coronal image. *ΔSI* was calculated from $\Delta SI=SI_{sample}-SI_{water}$, *ΔSI-C* curve was fitted using linear regression analysis in SPSS 13.0 statistical software.

1.2 Animal experiments

1.2.1 Solution preparation

Gd-DTPA was diluted with double distilled water into 10 mmol L^{-1}.

1.2.2 Experimental animals

Eight mature age-matched male Sprague Dawley rats weighing 250–300 g were used in the experiment. The animal protocols were approved by the Ethics Committee of Peking University Health Science Center (Approval No. LA 2009-008).

1.2.3 MR pre-scanning

All the rats (n=8) were anesthetized by an intraperitoneal injection of a combination of pentobarbital sodium, ethanol, chloral hydrate, magnesium sulphate and propylene glycol (3 mL kg^{-1}), and placed in a wrist coil and scanned by the MR system (Magnetom Trio, Siemens Medical Solutions, Erlangen, Germany) with a T_1-weighted three-dimensional magnetization prepared-rapid acquisition gradient echo (T_1 3D MP-RAGE) sequence.

1.2.4 Introduction of Gd-DTPA

Skin overlying the calvaria was shaved and disinfected with iodated alcohol. An incision was then made in the scalp along the sagittal suture, from the interaural area to the interocular area. The meninges were dissected and then the bregma was exposed. The rats were fixed in the stereotactic coordinate system (Lab Standard Stereotaxic-Single, Stoelting Co, Illinois, USA). According to the results of MR pre-scanning, a small trephine hole was made, 2 μL of solution with 10 mmol L^{-1} Gd-DTPA was microinjected (over a 10 min period) into the caudate nucleus [10]. Core temperature was monitored with a rectal thermometer and maintained with a heating pad at (~38±0.5)°C.

1.2.5 MR scanning

MR scanning was performed at different time intervals (1, 2, 3, 4, 6, 9 and 12 h) after the introduction of Gd-DTPA. The imaging sequence and parameters were the same as given before.

1.3 Image processing and quantitative calculation

A signal subtraction image was obtained by subtracting the pre-scan images from the post-scan images with MATLAB 7.8 software (MathWorks, Natick, MA). The signal intensity measured on the signal subtraction image was the signal intensity change (*ΔSI*). Then, all of the *ΔSI* values were converted into concentration values according to the *ΔSI-C* standard curve. Measurements were taken along three perpendicular axes, with the x-axis defined in the mediolateral direction, the y-axis as ventrodorsal, and the z-axis as rostrocaudal. A software program (unpublished), based on the modified diffusion equation, was included in the computation of the diffusion parameters.

When the scale of interest extended over several cellular dimensions in the brain ECS, extracellular diffusion was often described macroscopically as follows [2]:

$$\frac{\partial C_{ECS}}{\partial t}=\frac{D}{\lambda^2}\nabla^2 C_{ECS}+\frac{Q}{\alpha}-v\cdot\nabla C_{ECS}-\frac{f\left(C_{ECS}\right)}{\alpha}. \quad (1)$$

In eq. (1), the volume fraction α was defined as the ratio of the extracellular volume available for molecular diffusion in the compartment compared to the total tissue volume. Tortuosity was defined as $\lambda=(D/D^*)^{1/2}$, where D was the apparent diffusion coefficient of a given molecule in the brain ECS and D^* was the diffusion coefficient of the same molecule in a free solution. λ was a measure of how much the ECS structure hinders extracellular diffusion. C_{ECS} was the actual ECS concentration, t was the diffusion time, Q was the source function of the concentration. v represents the flow rate of the interstitial fluid in the ECS in mm s^{-1}. ∇

and ∇^2 symbolized respectively the first and the second spatial derivatives in the appropriate coordinate system, and $f(C_{\mathrm{ECS}})$ described the concentration clearance processes.

As interstitial fluid in the ECS channels was non-directional, the impact of bulk flow could be ignored. Eq. (1) was transformed to

$$\frac{\partial C_{\mathrm{ECS}}}{\partial t}=\frac{D}{\lambda^2}\nabla^2 C_{\mathrm{ECS}}+\frac{Q}{\alpha}-\frac{f\left(C_{\mathrm{ECS}}\right)}{\alpha}. \tag{2}$$

In the following text the term 'source' refers to the initial concentration available for diffusion or, in the case of an exogenous tracer such as Gd-DTPA, it refers to the site of the injection. Because there wasn't a constant input to the system and Gd-DTPA was assumed to have been administered at the original time point, the source Q could be ignored such that

$$\frac{\partial C_{\mathrm{ECS}}}{\partial t}=D^*\nabla^2 C_{\mathrm{ECS}}-\frac{f(C_{\mathrm{ECS}})}{\alpha}, \tag{3}$$

where $f(C_{\mathrm{ECS}})$ represented clearance of molecules out of the ECS, loss via capillaries, nonspecific uptake into cells, penetration backwards across the blood-brain barrier, drainage into extracranial lymphatic system, degradation by enzymes and other biochemical interactions with the extracellular matrix.

In the simplest case, diffusion of a substance in a medium was totally dependent on the concentration gradient between the source and surrounding medium, and $f(C_{\mathrm{ECS}})$ was proportional to the local concentration in the ECS. This means that

$$f(C_{\mathrm{ECS}})=-k'C_{\mathrm{ECS}}, \tag{4}$$

where k' was a first-order clearance rate constant (s^{-1}).

According to the equation $\Delta SI=kC=kC_{\mathrm{ECS}}\cdot\alpha$ (C referred to the average concentration of Gd-DTPA in the brain tissue) [20], Gd-DTPA in other spaces except ECS was assumed to have no contribution to the ΔSI measured on MR images. The linear relationship between the MR signal increment and Gd-DTPA concentration in the ECS was

$$C_{\mathrm{ECS}}=\frac{\Delta SI}{\alpha\cdot k}. \tag{5}$$

Substituting C_{ECS} in eq. (3) with that in eq. (5), we obtained

$$\frac{\partial\left(\frac{\Delta SI}{\alpha k}\right)}{\partial t}=D^*\nabla^2\left(\frac{\Delta SI}{\alpha k}\right)+k'\left(\frac{\Delta SI}{\alpha k}\right). \tag{6}$$

Dividing by αk, eq. (6) can be transformed to

$$\frac{\partial(\Delta SI)}{\partial t}=D^*\nabla^2(\Delta SI)+k'(\Delta SI). \tag{7}$$

The effective diffusion coefficient (D^*) and k' were estimated as follows.

Assuming a radial distribution in a system with spherical symmetry, eq. (7) becomes

$$\frac{\partial\Delta SI}{\partial t}=D\frac{1}{r^2}\frac{\partial}{\partial r}\left(r^2\frac{\partial(\Delta SI)}{\partial r}\right)+k'(\Delta SI), \tag{8}$$

where r is the distance extending from the original injection site to an arbitrary point along the direction used for the measurement. If it is assumed that there was no leakage through the boundary outlined by the edge of the diffusion pattern, then the analytic solution of eq. (8) becomes [11]

$$\Delta SI(t,r)=\sum_{n=0}^{\infty}\zeta_n\frac{\sin(\upsilon_n r)}{r}e^{-(\upsilon_n^2 D^*+k')t}, \tag{9}$$

where the expansion coefficient ζ_n is

$$\zeta_n=\frac{2\int_0^{r_0}\Delta SI_{,\mathrm{init}}(r)\sin(\upsilon_n r)r\mathrm{d}r}{r_0\left(1-\frac{\sin^2(\upsilon_n r_0)}{\upsilon_n^2 r_0^2}\right)}, \tag{10}$$

and r_0 is the radial size of the volume. The eigenvalue, υ_n, satisfied the eigenvalue equation, $\tan(\upsilon_n r_0)=\upsilon_n r_0$, and $\Delta SI_{,\mathrm{init}}(r)$ was the initial radial concentration profile.

The initial radial concentration, $\Delta SI_{,\mathrm{init}}(r)$, could be measured by averaging the MR signal profile from several different radial traces on the MR images acquired immediately after the injection. As time progressed, the model radial profile could be calculated using eq. (9). At time t_i and radius r, the MR signal increment is $\Delta SI(t_i,r)$.

As a series of MR images were captured at predetermined time intervals, t_i (i=1, 2,…,n), the radial profile along a given radial path for each MR image could be measured. The measured radial profile at time t_i was denoted as $\Delta SI_{,\mathrm{m}}(t_i,r)$.

In principle, the diffusion parameters D^* and k', can be measured by matching the model and measured profiles at time points t_i. Such "matching" processes were performed by using the standard least square fitting technique, where the sum of the squares of the differences between the model's predicted profiles and the measured profiles was minimized. For example, the following χ was minimized to find D^* and k'.

$$\chi=\sum_{i=1}^{N}\int_0^{r_0}\left(\Delta SI(t_i,r)-\Delta SI_{,\mathrm{m}}(t_i,r)\right)^2\mathrm{d}r, \tag{11}$$

where the error of the measured profile was assumed to be the same for all data points. In the computation of χ, the integration over radius, r, was replaced by a summation along a given path, along which the measurements were made from the injection site. A simplex-downhill method was used to perform the numerical minimization.

A software program (unpublished), based on the modified diffusion equation and the standard least square fitting technique, was employed in the computation of the diffusion parameters. The 3D MR series of images were imported to the program after post-processing. It was essential to choose a target point as the origin of diffusion, which was generally set in the center of the distribution zone of Gd-DTPA on MR images. Then the parameters were automatically computed for each pixel located 1–3 mm from the selected original site within the distribution area of Gd-DTPA labeling on MR images. The results were shown voxel-by-voxel on the converted images. Both the directions parallel and opposite to the three perpendicular axes were selected to present the diffusion parameters. The direction along + *y*-axis was excluded because of the interference by the needle track. For each direction, the diffusion parameters were designated to be from the voxel situated in the midpoint of the metrical radius (i.e., 2 mm from the original point). Parameters measured in the above five directions were then recorded for each rat.

1.4 The drainage, distribution and elimination process of the tracer in ISF

Initial image post-processing operations such as motion correction and coregistration were performed by a software program (unpublished) within MATLAB 7.8 based on an efficient mutual information method [12,13]. Then the profile of the diffusive pattern was automatically outlined on the MR subtracted images at different time scales by the software. The principle of the distribution and elimination for the tracer was intuitively analyzed on the dynamic MR images.

1.5 Statistical analysis

Statistical analysis was performed by SPSS 13.0. One-way analysis of variance (ANOVA) followed by individual comparisons of means was used for the comparison of parameters acquired in distinct directions. A paired-samples *t* test was used for the comparison of grouped data in the opposite directions.

2 Results

2.1 Linear relationship between *ΔSI* and Gd-DTPA concentration

A good linear relationship between *ΔSI* and Gd-DTPA concentration existed over the concentration range of 0–1 mmol L^{-1} (Figure 1). The linear equation was ΔSI=1475.0*C*, and the goodness of fit (R^2) was 0.985.

2.2 Diffusion pattern of Gd-DTPA after introduction into the rat brain

The MR signal of the caudate nucleus increased after Gd-DTPA was introduced into the brain (Figure 2). Gd-DTPA molecules diffused to the ipsilateral frontotemporal cortex over a period of 1–2 h. The MR signal intensity began to gradually attenuate at 2 h after the introduction of Gd-DTPA. The local deposition of Gd-DTPA in the caudate nucleus did not disappear until 12 h. With the enhancement area extracted on Figure 3, it was demonstrated that the tracer was transported by the drainage of CSF to the subarachnoid space around bilateral olfactory bulbs.

2.3 The quantification of diffusion properties

The concentration versus time profile is shown in Figure 4. The diffusive coefficient of Gd-DPTA molecules in the cerebral ECS of caudate nucleus is $(3.38\pm1.07)\times10^{-4}$ mm^2 s^{-1} (ANOVA, F=2.835, P=0.039<0.05). D^* was $(4.01\pm 0.60)\times 10^{-4}$ mm^2 s^{-1} in the caudate direction, and was significantly greater than the value measured in the cranial direction ($(2.54\pm1.27)\times10^{-4}$ mm^2 s^{-1}) (t=–3.159, P=0.016< 0.05). The clearance rate constant (k') calculated in various directions was invariant: ($(7.60\pm4.18)\times10^{-5}$ s^{-1}) (ANOVA, F=0.032, P=0.998>0.05). D^* measured in the cortex was $(1.66\pm0.81)\times10^{-5}$ mm^2 s^{-1}.

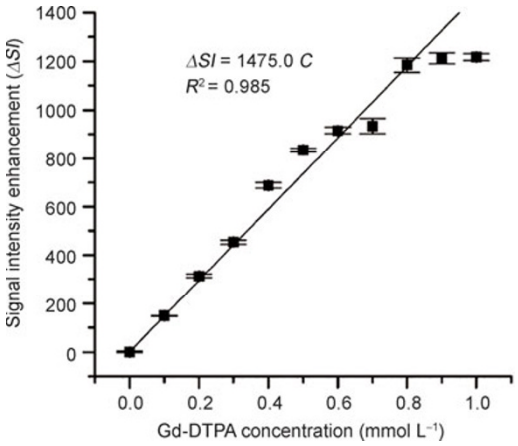

Figure 1 The Δ*SI*-*C* standard curve.

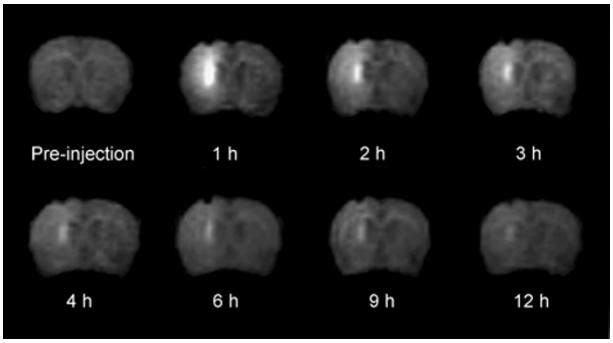

Figure 2 The diffusion of Gd-DTPA is shown on MRI at different time scales (coronary views). The enhancement in the rat brain is presented as hyperintensity (white) on the images.

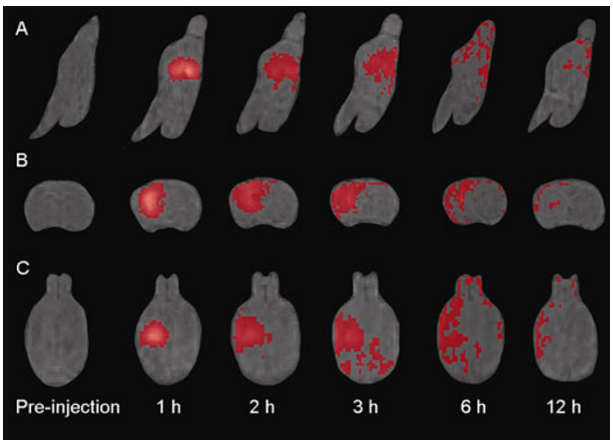

Figure 3 MRI appearances of the rat brain at different times after the injection of Gd-DTPA into the caudate nucleus. A, Sagittal views. B, Coronary views. C, Transverse views. 1 h, the deposition of the tracer is localized in a limited area around the injection spot; 2–3 h, the tracer extended to the ipsilateral cortex, then dispersed in the subarachnoid space close to the vertical surface of the brain; 6 h, migration of the tracer molecules was driven mainly by the flow of CSF in the cranial direction, and enhancement was presented in the subarachnoid space around bilateral olfactory bulbs; 12 h, the tracer was drained out of the brain by the ISF and CSF.

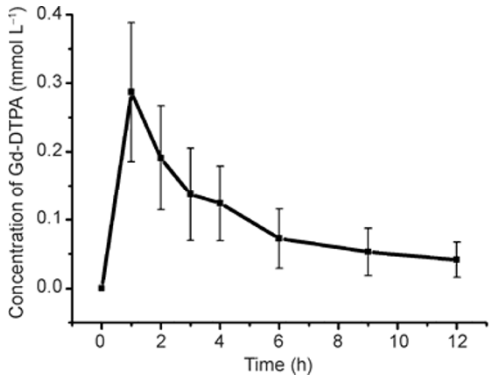

Figure 4 The concentration time-courses of Gd-DTPA in the rat brain. The measurement was performed in a voxel 2 mm to the original injection point in the caudate nucleus along the mediolateral direction. Parameters for the selected voxel were D^*=3.05×10^{-4} mm^2 s^{-1}, k'=7.59×10^{-5} s^{-1}.

3 Discussion

An *in vivo* measurement should be the basic requirement for any functional or physiological study of living organs, and is the key to ending the speculation and controversy regarding the nature of brain ISF. Although several techniques have been developed to measure the biophysical properties of the space around ISF (ECS), such as early studies with the radiotracer method [14], the RTI method using small ions [15,16] and integrative optical imaging (IOI) by macromolecular fluorescent substance [17], the observation of the drainage of ISF in living brain is not available and the diffusion properties of brain ECS can be determined only within a very short distance or a limited thickness [4].

The hydrophilic Gd-DTPA we used in the present study cannot enter cells, and the gadolinium ion buried in the cage is unlikely to bind to donor groups in proteins and enzymes [18,19]. Furthermore, a good linear relationship has been established between the Gd-DTPA induced MRI signal increment (ΔSI) and the concentration of Gd-DTPA below 1 mmol L^{-1} [20]. The amount and concentration of Gd-DTPA within brain tissue can therefore be accurately quantified. Comparing with the RTI method, the Gd-DTPA based MRI method provides not only an effective way of measuring the diffusion properties in the whole brain on a time scale of hours, the drainage of ISF was also visualized and discovered dynamically *in vivo*. With the caudate nucleus as the original injection point, a one-way drainage of brain ISF has been demonstrated from caudate nucleus towards frontal-temporal cortex.

Previous studies have suggested that ISF drains out of the brain along blood vessel walls [21]. A study using I^{125} serum albumin as a tracer verified that drainage of the ISF and solutes continues along the tunica media and tunica adventitia of the intracranial arteries [22]. The basement membranes in the walls of capillaries and arteries act as an important component of the pathway for drainage of ISF from the brain [23]. However, our present study verified that the distribution of tracer in the ISF is not strictly confined to the territory of the brain artery supply. The tracer reached most of the middle cerebral artery and part of the anterior cerebral artery territory, while no tracer was found in the internal regions of the frontal lobe and its distal olfactory bulbs (Figure 2).

The tracer injected into the brain cortex extended bilaterally and did not flow towards the caudate nucleus (the results were not shown). Also, the tracer did not flux backward or inferiorly to the thalamus region, which demonstrated that the ISF within the ECS drains in a one-way pattern and the distribution is not confined to any known specialized anatomical division, such as the brain artery supply territory [24,25] or fiber projection pathway [26,27].

The tracer drained to the subarachnoid space at 3 h as it reached the brain cortex, after which it flowed towards the frontal regions and finally surrounded bilateral olfactory bulbs. Although the nasal region was not the imaging target in our current study, the distribution of tracer within the subarachnoid space was consistent with the study of Muldoon *et al.* [28], which verified the clearance pathway of ISF to cervical deep lymph nodes via nasal lymphatics.

According to the fact that ECS occupies a much higher volume fraction (20%) than the brain microvessels (3%) in the whole brain [2], some researchers have developed innovative drug delivery techniques via ECS channels to circumvent the blood-brain barrier, Bobo *et al*. proposed the CED in 1994 [29] and more recently, Han *et al*. [7] proposed and validated a less invasive delivery method named SDD in 2011 [30]. By using CED and SDD, therapeutic agents can distribute and achieve drug concentrations that are orders of magnitude greater than systemic levels.

A study using confocal microscopy suggested that the drainage of the solutes, 3-kD dextran and 40-kD ovalbumin

included two phases: initially by diffusion through the ECS and then by perivascular drainage along the basement membranes of capillaries and arteries. Our results cannot discriminate the micro-localization of the tracer, because the basic unit of the MR image is the voxel with a minimum size of 0.125 mm^3. Although the derived diffusion parameter was an average of diffusion parameters of all brain ECS within one voxel, it could enable visualization of the drainage and distribution of brain ISF. In the present study, the diffusion parameters of a voxel at 2 mm lateral to the original injection point was derived as $(3.38\pm1.07)\times10^{-4}$ mm^2 s^{-1}. This means that the tracer will distribute within a radius of (0.88±0.58) mm in 2 h, although the distance from the selected voxel to the edge of the cortex is (1.66±0.51) mm. Therefore, both diffusion and bulk flow contribute to the drainage of ISF. By using a mathematical model, Schley *et al*. also deduced that perivascular transport of solutes out of the brain was driven by the bulk flow of ISF [23].

Either diffusion or bulk flow (convection) can be used to enhance the transport of drugs within the brain ECS. For CED, a continuous positive-pressure infusion was used to enhance the convection of drug delivery [9], while, with SDD, the transport of drugs with a small molecular weight can be realized only under the concentration gradient, by which the drug diffuses within brain ECS and then is driven to the target region along the drainage pathway by self-diffusion and bulk flow of the ISF. With this newly developed quantitative imaging method, we believe that further understanding of the nature of ISF *in vivo* will be followed by a full flourishing of drug therapy via the brain interstitium.

This work was supported by the National Natural Science Foundation of China (Grant Nos. 30972811, 81171080 and 81071148) and the Twelfth Five-year Plan for National Science and Technology of China (Grant No. 2012BAI15B009).

1 Abbott N J. Evidence for bulk flow of brain interstitial fluid: significance for physiology and pathology. Neurochem Int, 2004, 45: 545–552
2 Sykova E, Nicholson C. Diffusion in brain extracellular space. Physiol Rev, 2008, 88: 1277–1340
3 Nicholson C, Phillips J M. Ion diffusion modified by tortuosity and volume fraction in the extracellular microenvironment of the rat cerebellum. J Physiol, 1981, 321: 225–257
4 Nicholson C, Sykova E. Extracellular space structure revealed by diffusion analysis. Trends Neurosci, 1998, 21: 207–215
5 Nicholson C. Factors governing diffusing molecular signals in brain extracellular space. J Neural Transm, 2005, 112: 29–44
6 Kunwar S, Chang S, Westphal M, *et al*. Phase III randomized trial of CED of IL13-PE38QQR vs Gliadel wafers for recurrent glioblastoma. Neuro Oncol, 2010, 12: 871–881
7 Han H, Xia Z, Chen H, *et al*. Simple diffusion delivery via brain interstitial route for the treatment of cerebral ischemia. Sci China Life Sci, 2011, 54: 235–239
8 Bidros D S, Liu J K, Vogelbaum M A. Future of convection- enhanced delivery in the treatment of brain tumors. Future Oncol, 2010, 6: 117–125
9 Lopez K A, Waziri A E, Canoll P D, *et al*. Convection-enhanced delivery in the treatment of malignant glioma. Neurol Res. 2006, 28: 542–548
10 Paxinos G, Watson C. The rat brain in stereotaxic coordinates. 6th ed. London: Academic Press, 2007. 80–84
11 Koshlyakov N S, Smirnov M M, Gliner E B. Differential equations of mathematical physics. Amsterdam: North-Holland Publishing Co., 1964. 509
12 Pluim J P W, Maintz J B A, Viergever M A. Mutual-information-based registration of medical images: a survey. IEEE Trans Med Imag, 2003, 22: 986–1004
13 Loeckx D, Slagmolen P, Maes F, *et al*. Nonrigid image registration using conditional mutual information. IEEE Trans Med Imag, 2010, 29: 19–29
14 Patlak C S, Hospod F E, Trowbridge S D, *et al*. Diffusion of radiotracers in normal and ischemic brain slices. J Cereb Blood Flow Metab, 1998, 18: 776–802
15 Ransom B R, Yamate C L, Connors B W. Activity-dependent shrinkage of extracellular space in rat optic nerve: a developmental study. J Neurosci, 1985, 5: 532–535
16 Nicholson C. Quantitative analysis of extracellular space using the method of TMA^+ iontophoresis and the issue of TMA^+ uptake. Can J Physiol Pharmacol, 1992, 70: S314–S322
17 Nicholson C, Tao L. Hindered diffusion of high molecular weight compounds in brain extracellular microenvironment measured with integrative optical imaging. Biophys J, 1993, 65: 2277–2290
18 Cabella C, Crich S G, Corpillo D, *et al*. Cellular labeling with Gd(III) chelates: only high thermodynamic stabilities prevent the cells acting as 'sponges' of Gd^{3+} ions. Contrast Media Mol Imaging, 2006, 1: 23–29
19 Caravan P, Ellison J J, Mcmurry T J, *et al*. Gadolinium(III) chelates as MRI contrast agents: structure, dynamics, and applications. Chem Rev, 1999, 99: 2293–2352
20 Xu F, Han H, Zhang H, *et al*. Quantification of Gd-DTPA concentration in neuroimaging using T_1 3D MP-RAGE sequence at 3.0 T. Magn Reson Imaging, 2011, 29: 827–834
21 Weller R O, Galea I, Carare R O, *et al*. Pathophysiology of the lymphatic drainage of the central nervous system: implications for pathogenesis and therapy of multiple sclerosis. Pathophysiology, 2010, 17: 295–306
22 Yamada S, Depasquale M, Patlak C S, *et al*. Albumin outflow into deep cervical lymph from different regions of rabbit brain. Am J Physiol, 1991, 261: H1197-H1204
23 Schley D, Carare-Nnadi R, Please C P, *et al*. Mechanisms to explain the reverse perivascular transport of solutes out of the brain. J Theor Biol, 2006, 238: 962–974
24 Yamori Y, Horie R, Handa H, *et al*. Pathogenetic similarity of strokes in stroke-prone spontaneously hypertensive rats and humans. Stroke, 1976, 7: 46–53
25 Tamura A, Graham D I, Mcculloch J, *et al*. Focal cerebral ischaemia in the rat: 1. Description of technique and early neuropathological consequences following middle cerebral artery occlusion. J Cereb Blood Flow Metab, 1981, 1: 53–60
26 Berendse H W, Galis-De G Y, Groenewegen H J. Topographical organization and relationship with ventral striatal compartments of prefrontal corticostriatal projections in the rat. J Comp Neurol, 1992, 316: 314–347
27 Berendse H W, Groenewegen H J, Lohman A H. Compartmental distribution of ventral striatal neurons projecting to the mesencephalon in the rat. J Neurosci, 1992, 12: 2079–2103
28 Muldoon L L, Varallyay P, Kraemer D F, *et al*. Trafficking of superparamagnetic iron oxide particles (Combidex) from brain to lymph nodes in the rat. Neuropathol Appl Neurobiol, 2004, 30: 70–79
29 Bobo R H, Laske D W, Akbasak A, *et al*. Convection-enhanced delivery of macromolecules in the brain. Proc Natl Acad Sci USA, 1994, 91: 2076–2080
30 Xu F, Han H, Yan J, *et al*. Greatly improved neuroprotective efficiency of citicoline by stereotactic delivery in treatment of ischemic injury. Drug Deliv, 2011, 18: 461–467